




Article

Chemical Synthesis, Proper Folding, Na_v Channel Selectivity Profile and Analgesic Properties of the Spider Peptide Phlotoxin 1

Sébastien Nicolas ^{1,†}, Claude Zoukimian ^{2,3,†}, Frank Bosmans ^{4,5,†}, Jérôme Montnach ¹, Sylvie Diochot ⁶, Eva Cuypers ⁵, Stephan De Waard ¹, Rémy Bérout ², Dietrich Mebs ⁷ , David Craik ⁸, Didier Boturyn ³ , Michel Lazdunski ⁶, Jan Tytgat ⁵ and Michel De Waard ^{1,2,*} 

¹ Institut du Thorax, Inserm UMR 1087/CNRS UMR 6291, LabEx “Ion Channels, Science & Therapeutics”, F-44007 Nantes, France; sebastien.nicolas@univ-nantes.fr (S.N.); jerome.montnach@univ-nantes.fr (J.M.); stephan.de-waard@etu.univ-nantes.fr (S.D.W.)

² Smartox Biotechnology, 6 rue des Platanes, F-38120 Saint-Egrève, France;

Claude.Zoukimian@univ-grenoble-alpes.fr (C.Z.); remy.beroud@smartox-biotech.com (R.B.)

³ Department of Molecular Chemistry, Univ. Grenoble Alpes, CNRS, 570 rue de la chimie, CS 40700, 38000 Grenoble, France; didier.boturyn@univ-grenoble-alpes.fr

⁴ Faculty of Medicine and Health Sciences, Department of Basic and Applied Medical Sciences, 9000 Gent, Belgium; frank.bosmans@ugent.be

⁵ Toxicology and Pharmacology, University of Leuven, Campus Gasthuisberg, P.O. Box 922, Herestraat 49, 3000 Leuven, Belgium; eva.cuypers@kuleuven.be (E.C.); jan.tytgat@kuleuven.be (J.T.)

⁶ Université Côte d’Azur, CNRS UMR7275, Institut de Pharmacologie Moléculaire et Cellulaire, 660 route des lucioles, 6560 Valbonne, France; diochot@ipmc.cnrs.fr (S.D.); lazdunski@ipmc.cnrs.fr (M.L.)

⁷ Institute of Legal Medicine, University of Frankfurt, Kennedyallee 104, 60488 Frankfurt, Germany; mebs@em.uni-frankfurt.de

⁸ Institute for Molecular Bioscience, University of Queensland, Brisbane 4072, Australia; d.craik@imb.uq.edu.au

* Correspondence: michel.dewaard@univ-nantes.fr; Tel.: +33-228-080-076

† Contributed equally to this work.

Received: 16 May 2019; Accepted: 16 June 2019; Published: 21 June 2019



Abstract: Phlotoxin-1 (PhlTx1) is a peptide previously identified in tarantula venom (*Phlogius* species) that belongs to the inhibitory cysteine-knot (ICK) toxin family. Like many ICK-based spider toxins, the synthesis of PhlTx1 appears particularly challenging, mostly for obtaining appropriate folding and concomitant suitable disulfide bridge formation. Herein, we describe a procedure for the chemical synthesis and the directed sequential disulfide bridge formation of PhlTx1 that allows for a straightforward production of this challenging peptide. We also performed extensive functional testing of PhlTx1 on 31 ion channel types and identified the voltage-gated sodium (Na_v) channel Na_v1.7 as the main target of this toxin. Moreover, we compared PhlTx1 activity to 10 other spider toxin activities on an automated patch-clamp system with Chinese Hamster Ovary (CHO) cells expressing human Na_v1.7. Performing these analyses in reproducible conditions allowed for classification according to the potency of the best natural Na_v1.7 peptide blockers. Finally, subsequent *in vivo* testing revealed that intrathecal injection of PhlTx1 reduces the response of mice to formalin in both the acute pain and inflammation phase without signs of neurotoxicity. PhlTx1 is thus an interesting toxin to investigate Na_v1.7 involvement in cellular excitability and pain.

Keywords: spider toxin; directed disulfide bond formation; Na_v channel activity; Na_v1.7; pain target; automated patch-clamp

Key Contribution: This manuscript describes the first complete chemical synthesis of phlotoxin 1 that uses a directed disulfide bond formation strategy. Thanks to the synthetic product, phlotoxin 1

activity could be fully characterized with regard to its selectivity profile on K_v and Na_v channels, and its potency could be ranked among other toxins active on $Na_v1.7$; an important pain target.

1. Introduction

Voltage-gated sodium (Na_v) channels are critical for the generation and propagation of action potentials [1–4]. They are composed of a pore-forming α -subunit and can be associated with β -subunits [5]. Nine isoforms of vertebrate α -subunits have been identified so far ($Na_v1.1$ to $Na_v1.9$), that can be further distinguished by their sensitivity to tetrodotoxin (TTX); a toxin from the Japanese Puffer fish. Indeed, $Na_v1.5$, 1.8 and 1.9 are TTX-resistant (TTX-r), whereas the other α -subunits are TTX-sensitive (TTX-s). These channels also differ by their distribution with $Na_v1.1$, 1.2 and 1.3 principally found in the central nervous system, whereas $Na_v1.6$, 1.7, 1.8 and 1.9 are predominantly, but not exclusively, expressed in the peripheral nervous system. In addition, $Na_v1.4$ is predominantly found within the skeletal muscle, whereas $Na_v1.5$ is chiefly present in cardiac muscle.

Na_v channels are involved in a wide array of physiological processes. In particular, $Na_v1.7$ was clearly identified as playing a crucial role in nociceptive pathways, which led to research into the development of novel therapeutics for pain treatment [6–18]. For examples, missense mutations of the *SCN9A* gene that encodes $Na_v1.7$ produces congenital indifference to pain [19]. Mice in which the *SCN9A* gene is inactivated produce a similar phenotype of pain resistance [20,21]. *A contrario*, gain of function mutations of *SCN9A* lead to the opposite spectra of clinical manifestations, including paroxysmal extreme pain disorder [22], painful small fiber neuropathy [23,24], idiopathic small fiber neuropathy [2,25], or primary erythromelalgia with burning pain in extremities [26–28]. A set of biophysical alterations in $Na_v1.7$ channel properties accompanies these pathologies, including changes in fast inactivation, the induction of persistent currents, and lower voltage thresholds for activation. Upregulation of $Na_v1.7$ is also associated with metastatic potential in prostate cancer in vivo and could therefore be used as a putative functional diagnostic marker [29,30]. Finally, $Na_v1.7$ may (i) have a role in the migration and cytokine responses of human dendritic cells [31]; (ii) help regulate neural excitability in vagal afferent nerves [32]; and (iii) contribute to odor perception in humans [33]. Despite its therapeutic potential, the task of identifying selective $Na_v1.7$ channel inhibitors remain challenging given the high level of sequence homologies among Na_v channel isoforms, particularly in the structural loci governing ion conduction and selectivity. In spite of these difficulties, Xenome Pharmaceuticals successfully discovered XEN402, a compound that exhibits a voltage-dependent block of $Na_v1.7$ and is capable of alleviating pain in erythromelalgia patients [34]. Researchers at Merck reported the discovery of a novel benzazepinone compound that blocks $Na_v1.7$ and is orally effective in a rat model of neuropathic pain [35]. Finally, Genentech investigators found that aryl sulfonamide inhibitors selectively block $Na_v1.7$ by a voltage-sensor trapping mechanism [36]. Due to their physiological importance, Na_v channels are also one of the foremost targets of animal venoms or plant neurotoxins [37–39]. The binding properties of peptide toxins have characteristic features that facilitate the identification of new Na_v channel isoform-selective pharmacological entities. For example, many of the peptidic toxins identified so far do not target the conserved pore region but rather act as gating modifiers by influencing movements of the less-conserved voltage-sensing domain within Na_v channels [40,41]. This feature further enhances the success rate for identifying $Na_v1.7$ blockers with substantially improved selectivity over other Na_v isoforms. Reports on high affinity toxins for $Na_v1.7$ that are efficient to treat pain remain infrequent. For instance, the tarantula venom peptide protoxin II (ProTx-II) potently inhibits $Na_v1.7$ activation and abolishes C-fiber compound action potentials in desheathed cutaneous nerves [42]. However, ProTx-II application has little effect on action potential propagation of an intact nerve, an observation that may explain why ProTx-II is not efficacious in rodent models of acute and inflammatory pain. The scorpion toxin OD1 impairs $Na_v1.7$ fast inactivation at low nanomolar concentrations but lacks the required Na_v channel isoform selectivity [43]. Finally,

μ -SLPTX-Ssm6a from centipede venom was reported to block $\text{Na}_v1.7$ -mediated currents and produce favorable analgesic activity in a rodent model of chemical-induced, thermal, and acid-induced pain [44]; however, these data have yet to be reproduced. Part of the lack of efficacy of toxins on pain treatment can be explained by the fact that they require a concomitant activation of the opioid system to reveal their analgesic properties [45]. The Theraphosidae family of spiders, belonging to the Mygalomorpha suborder, provided up to 20 analgesic peptides so far, all acting on $\text{Na}_v1.7$, and belong to one of three spider toxin families (NaSpTx-1, NaSpTx-2 and NaSpTx-3) [46]. All these peptides vary in size from 26 to 35 amino acid residues, and are folded according to an inhibitor cysteine knot architecture with three disulfide bridges organized in a Cys¹-Cys⁴, Cys²-Cys⁵, and Cys³-Cys⁶ pattern. As a rule, these peptides are difficult to fold and require expert chemical techniques for synthetic production. Altogether, because analgesic peptides are difficult to identify, it remains important to further enlarge the repertoire of $\text{Na}_v1.7$ -blocking toxins available to investigators interested in pain therapeutics.

Here, we report the chemical synthesis and the directed disulfide bridge formation of phlotoxin-1 (PhlTx1), a 34-residue and three disulfide-bridged toxin from the venom of a Papua New Guinea tarantula of a *Phlogiellus* genus spider species that was only scarcely characterized so far [47]. In addition, some synergistic effects were observed to occur between low doses of PhlTx1 and opioids for the treatment of inflammatory pain, suggesting an effect on $\text{Na}_v1.7$ channel [45,48]. Herein, PhlTx1 was tested on a large array of ion channels including voltage-gated potassium (K_v) channels, members of the two-pore domain potassium channel family (TASK1, TRAAK), inward-rectifying potassium channels, voltage-gated calcium (Ca_v) channels and Na_v channels expressed in either *Xenopus laevis* oocytes, COS or CHO cells. Remarkably, the principal effect was seen on Na_v channels. In particular, $\text{Na}_v1.7$ was found to represent the most sensitive isoform for PhlTx1 inhibition. We compared the $\text{Na}_v1.7$ blocking efficacy of PhlTx1 to 10 other-published $\text{Na}_v1.7$ blocking toxins that we chemically synthesized. Using an automated patch-clamp system with a single CHO expressing human $\text{Na}_v1.7$ cell line, we ranked the potency of PhlTx1 activity on human $\text{Na}_v1.7$ channel *versus* these other spider toxins in uniform experimental conditions. Finally, the analgesic potential of PhlTx1 was studied using the formalin pain test, indicating that it also represents an interesting lead compound for the development of an analgesic.

2. Results

2.1. PhlTx1 Description

PhlTx1 has been purified originally from the venom of *Phlogiellus* sp., *Theraphosidae Selenocosmiinae* (endemic to Papua New Guinea) and sequenced [47]. The peptide contains 34 amino acid residues, six cysteine residues bridged in an inhibitory cysteine-knot (ICK) architecture fold and is amidated at the C-terminus. The reported molecular weight of PhlTx1 is 4058.83 Da. Sequence alignment of PhlTx1 with other spider toxins illustrate that PhlTx1 has limited homology with previously identified peptides (sequence identities varying between 24 and 59% at best) (Figure 1). According to its sequence, PhlTx1 fits best within the NaSpTx-1 family with the following disulfide bridge organization: Cys²-Cys¹⁷, Cys⁹-Cys²², Cys¹⁶-Cys²⁹. In contrast, it has very little homology with toxins from NaSpTx-2, NaSpTx-3 and NaSpTx-7 families (Figure 1). Several structural features of PhlTx1 hint at difficulties performing chemical synthesis. First, it contains three Pro residues (Pro¹¹, Pro¹⁸ and Pro²⁷) that are all susceptible to trans/cis isomerization and hence influence the proper induction of the secondary structures as well as the appropriate disulfide bridge pattern. Second, the immediate proximity of Cys¹⁶ and Cys¹⁷ is potentially a factor that could lead to disulfide bridge disarrangement, accompanied by inappropriate folding of the peptide and altered pharmacology. Finally, the lack of reporting on the chemical synthesis of PhlTx1, in spite of its potential interest ($\text{Na}_v1.7$ target for pain treatment) and its discovery dating back to 2005 is a sign that its chemical synthesis is not straightforward.

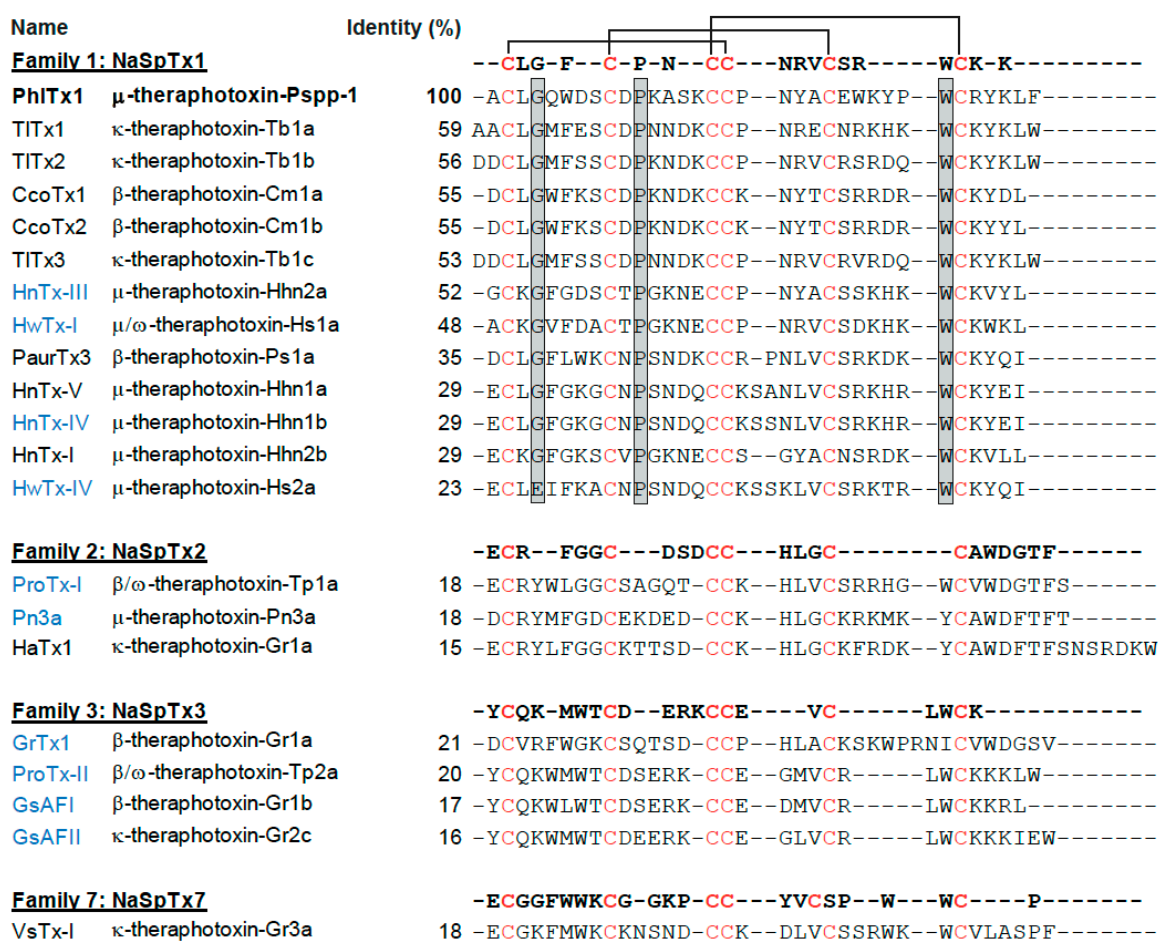


Figure 1. Sequence alignment of PhlTx1 with other spider toxins. Highly conserved cysteines are indicated in red and probable cysteine pairing, according to the inhibitory cysteine knot motif and the consensus sequence for NaSpTx-1 family of toxins, is indicated at the top with black lines. Percent conserved residues are indicated on the right. Shaded boxed residues correspond to the consensus residues of NaSpTx-1 toxin sequences. The lower homology with toxins from NaSpTx-2, NaSpTx-3 and NaSpTx-7 families are also shown. Toxins that are in blue have been compared in terms of activity on the Na_v1.7 channel with PhlTx1 (see Figure 7).

2.2. PhlTx1 Chemical Synthesis

In a first attempt to produce synthetic PhlTx1, the peptide was first stepwise assembled using fmoc chemistry, fully deprotected and purified from the crude synthetic products by preparative reversed-phase high pressure liquid chromatography (RP-HPLC) (Figure 2A). The purified linear peptide has the expected monoisotopic mass of 4061.79 (Figure 2A inset). Random oxidative folding of the peptide was performed at 0.1 mg/mL in a 100 mM Tris-HCl buffer at pH 8.4 with 5 mM reduced (GSH), 0.5 mM oxidized glutathione (GSSG) and 2 M Gn.HCl during 72 h at room temperature. According to the elution profile on RP-HPLC, the folding was (i) not straightforward, (ii) of very low yield and (iii) provided several peaks, possibly because of trans/cis isomerization properties of the Pro residues (data not shown). However, a dominant peak was purified as shown on the elution profile (Figure 2B). This purified peak resulted in the observation of two peaks in analytical RP-HPLC unless the column was heated, indicating the involvement of at least one Pro residue involved in trans/cis isomerization. Purifying either peak resulted in the production of the second peak demonstrating that the two forms (cis and trans) of the peptide are in equilibrium (data not shown). Other oxidative folded products may reflect misfolding of the peptide and inappropriate disulfide bridge arrangements. Purified folded/oxidized synthetic PhlTx1 was nevertheless shown to possess the proper monoisotopic

mass of 4055.74 Da (Figure 2B inset). The 6 Da reduction in molecular weight of PhlTx1 is consistent with the formation of three disulfide bridges, but does not provide any indication about the favored pattern of disulfide bridges adopted by the toxin during this oxidative folding.

Because the random oxidative folding strategy and the final yield of production of PhlTx1 seemed problematic, we tried a directed disulfide bond formation strategy that ensures that the proper disulfide bridges are formed as expected for a NaSpTx-1 family toxin. Three different protecting groups were used for the lateral chains of Cys residues: Trt for Cys⁹-Cys²², Acn for both Cys² and Cys¹⁷, and Mob for both Cys¹⁶ and Cys²⁹. The sequential order of disulfide bridge formation was thus Cys⁹-Cys²² first after a classical deprotection of Trt groups with TFA, followed by Cys²-Cys¹⁷ second and lastly Cys¹⁶-Cys²⁹ (Figure 2C). The two first disulfide bridges were sequentially formed in the same reaction buffer (one pot reaction), while the deprotection of Mob and the formation of the third disulfide bridge were done after purification of the two-disulfide-bridged PhlTx1. The synthetic crude PhlTx1 with the four remaining protecting groups (2 Acn and 2 Mob) after deprotection is shown on the RP-HPLC elution profile in Figure 2D, while the crude reaction mixture after formation of the first disulfide bridge is shown in Figure 2E. Formation of the first disulfide bridge is witnessed by the mass spectrometry analyses that illustrate a reduction in molecular weight (see insets; exact mass 4443.97 Da for the unfolded and 4441.96 Da for the one-disulfide bridged PhlTx1). The second disulfide bridge was formed after formation of the first one without intermediary purification in acidic conditions by the removal of the Acn protecting groups using iodine (see crude reaction mixture after formation of the second disulfide bridge in Figure 2F) and purified to homogeneity (Figure 2G). The acidic conditions were set to avoid disulfide bridge scrambling and secondary reactions with iodine such as iodine adducts on tyrosine or tryptophan residues. Next, the third disulfide bridge was formed in an oxidative and acidic buffer after removal of the Mob protecting groups with trifluoromethanesulfonic acid (TFMSA). Again, acidic conditions were used to avoid the risks of scrambling (see crude product in Figure 2H). The purified two-disulfide and three disulfide-bridged PhlTx1 are shown in Figure 2I. The large leftward shift observed in the retention time during elution is mainly due to the removal of the Mob protecting groups that are highly hydrophobic. All figure insets illustrating mass spectrometry profiles of the products indicate that each disulfide bridge has been formed properly with the appropriate removals of the protecting groups (exact mass of 4297.87 Da for the two disulfide-bridged PhlTx1 and 4055.73 Da for the fully-bridged disulfide PhlTx1). The overall yield of PhlTx1 production was 1.4%, which was 5 times better than that reached by random folding strategy. Nevertheless, the first strategy is expected to yield the same type of folding as both pure synthetic PhlTx1 coeluted perfectly (Figure 2J). This further illustrates that we purified the right peak within the random oxidative folding strategy, a fact that was not guaranteed in advance considering the presence of several peaks with the proper masses for oxidized PhlTx1. The directed disulfide bonding strategy we used should reveal itself to be very useful in experimental conditions where the random oxidative folding strategy turns to be inefficient (in SAR studies for example).

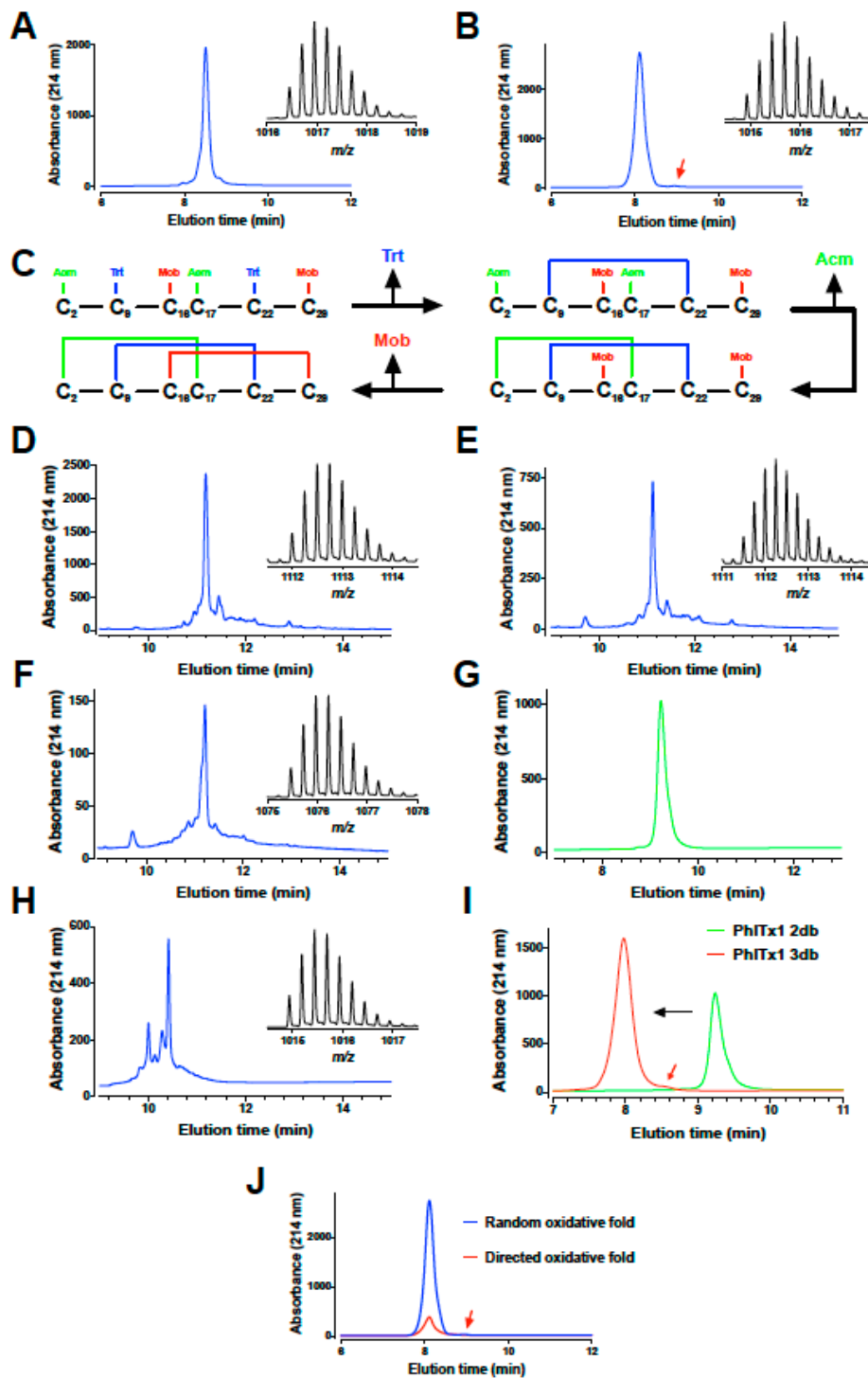


Figure 2. Comparative chemical synthesis of PhITx1 following the random oxidative folding or the directed disulfide bond formation strategies. (A) Analytical RP-HPLC of the purified linear PhITx1 meant to be produced by random oxidative folding (only Trt protecting groups for the 6 cysteine residues during chemical synthesis). Inset: MS spectrum of synthetic linear PhITx1. $[M + 4H]^{4+}$ of 1016.45. (B) Analytical RP-HPLC of the folded oxidized PhITx1. Red arrow possibly indicates the second conformer of PhITx1 that is present. Inset: MS spectrum of purified PhITx1. $[M + 4H]^{4+}$ of 1014.94. (C) Schematic procedure employed for the directed disulfide bond formation strategy. (D) Analytical RP-HPLC of the crude linear PhITx1 used for the directed disulfide bond formation strategy. Inset: MS spectrum of the synthetic compound with the Acm and Mob protecting groups. $[M + 4H]^{4+}$ of 1111.99. (E) Analytical RP-HPLC of crude PhITx1 with its first disulfide bridge. Inset: corresponding MS

spectrum of the compound. $[M + 4H]^{4+}$ of 1111.50. (F) Analytical RP-HPLC of crude PhlTx1 with its two first disulfide bridges. Inset: corresponding MS spectrum of the compound. $[M + 4H]^{4+}$ of 1075.47. (G) Analytical RP-HPLC of purified PhlTx1 with its two first disulfide bridges. (H) Analytical RP-HPLC of crude PhlTx1 in its fully folded configuration. Inset: corresponding MS spectrum of the compound. $[M + 4H]^{4+}$ of 1014.94. (I) (G) Analytical RP-HPLC of purified two-disulfide bridged (2db) and three-disulfide-bridged (3db) PhlTx1 to illustrate the important reduction of hydrophobicity of the peptide upon removal of the Mob protecting groups. (J) Coelution of purified PhlTx1 produced by random oxidative folding with that produced by a directed disulfide bond formation strategy.

2.3. Ion Channel Selectivity of PhlTx1 and Preferential Activity on $Na_v1.7$

We tested the biological activity of PhlTx1 on a large selection of ion channels that comprise K_v channels, two members of the two-pore domain potassium channel family (TASK1, TREK2), inward-rectifying potassium channels, the acetylcholine receptor and Na_v channels (Figure 3). All tested targets were heterologously expressed in either *Xenopus laevis* oocytes and/or COS cells and the resulting ionic currents were measured using electrophysiological voltage-clamp techniques. When applying 1 μ M PhlTx1 to all tested ion channels and measuring current inhibition at the voltage of maximum ion flux, $K_v3.4$ was the only non- Na_v channel impacted by the toxin (significant inhibition close to 20%). None of the channels tested were activated by the toxin.

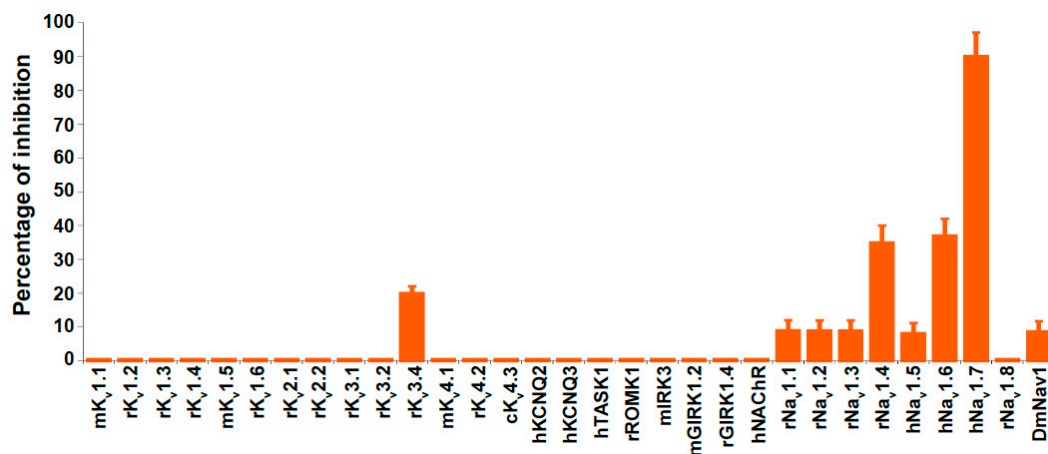


Figure 3. Overview of all tested channels indicating the percentage inhibition upon application of 1 μ M PhlTx1. Expression system was either *Xenopus laevis* oocytes (all Na_v channels) and/or COS cells. Estimation of the effect on nicotinic acetylcholine receptor NAChR was achieved by 125 I- α -bungarotoxin binding as previously described [49]. Clones were from the following species: m, mouse; r, rat; c, canine; h, human; and Para/tipE, Fruit fly.

Using the two-electrode voltage-clamp technique on *Xenopus laevis* oocytes, the effect of PhlTx1 was also compared on eight different cloned vertebrate Na_v channels co-expressed with the β_1 subunit ($Na_v1.1$ - $1.8/\beta_1$) and on the neuronal insect Na_v channel, para, co-expressed with the tipE subunit (Figures 3 and 4). When measured at the voltage of maximum sodium influx from a holding potential of -90 mV, 1 μ M of PhlTx1 marginally decreased the sodium currents (10%) of most Na_v channel subtypes, while $Na_v1.8/\beta_1$ was not inhibited. Conversely, $Na_v1.4/\beta_1$ and $Na_v1.6/\beta_1$ currents revealed a maximum reduction of 35% when 1 μ M PhlTx1 was applied (Figure 3). However, the inward currents of $Na_v1.7/\beta_1$ were almost completely inhibited ($90 \pm 7\%$) at 1 μ M (Figure 3). Normalized current-voltage relationships (I-V curve) of $Na_v1.2/\beta_1$ and $Na_v1.3/\beta_1$ channels seemed to be shifted towards more negative potentials when PhlTx1 was applied, but shifts were not statistically significant ($p < 0.05$) (Figure 4). The activation phase of the other studied Na_v channel subtypes was not affected. No obvious alteration in channel availability was observed, except a 5-mV negative shift for $Na_v1.3/\beta_1$, although that was also non-significant ($p > 0.05$).

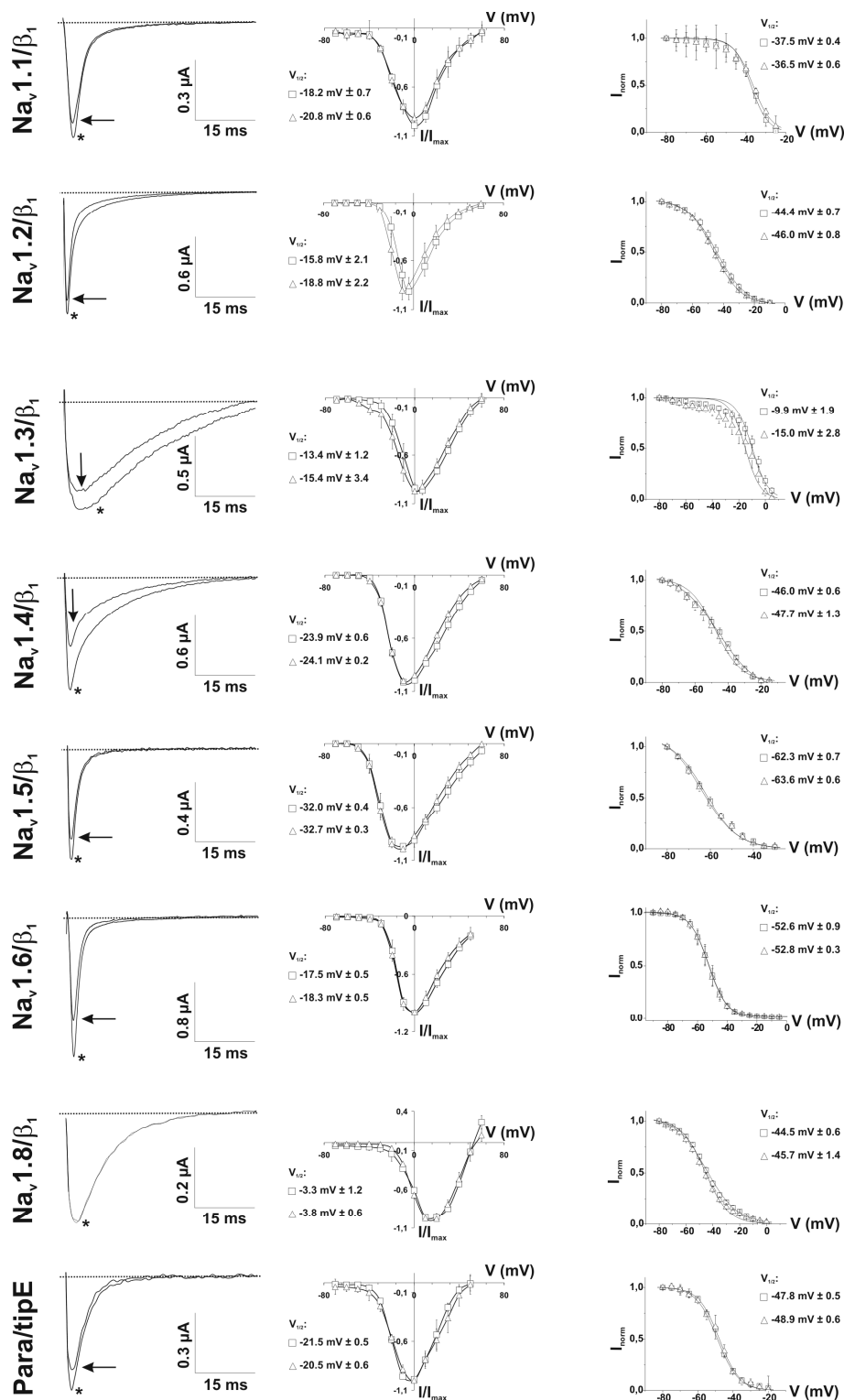


Figure 4. 1 μ M of PhlTx1 was tested on $Na_v1.1/\beta_1$, $Na_v1.2/\beta_1$, $Na_v1.3/\beta_1$, $Na_v1.4/\beta_1$, $Na_v1.5/\beta_1$, $Na_v1.6/\beta_1$, $Na_v1.8/\beta_1$ and para/tipE ($n \geq 3$). Left column: current traces were evoked by a 50-ms depolarization to the voltage of maximum sodium influx, depending on the Na_v studied, from a holding potential of -90 mV. At 1 μ M PhlTx1, all studied Na_v channels, except $Na_v1.4/\beta_1$, were blocked for about 10% (no toxin: *). The current of $Na_v1.4/\beta_1$ was reduced for about $35 \pm 5\%$. Middle column: normalized I-V curves reveal no significant shift of the activation voltage ($p > 0.05$). Symbols: (\square) before and (Δ) after addition of 1 μ M PhlTx1. Right column: steady-state inactivation curves for all studied Na_v isoforms. No significant shift was observed for any of the channels ($p < 0.05$).

We further characterized the inhibition of $\text{Na}_v1.7/\beta_1$ currents by PhlTx1. The residual inward current after at 1 μM PhlTx1 addition seems to occur without any alteration in channel kinetics (Figure 5A). Outward sodium currents at depolarizing voltages (+100 mV) were also blocked, as assayed with the help of tetrodotoxin (TTX; 50 nM) which physically occludes the pore (Figure 5B). Furthermore, $\text{Na}_v1.7/\beta_1$ inhibition did not seem to be very voltage-dependent, since the reduction of sodium currents at more hyperpolarized voltages (−70 to −30 mV) was similar to the reduction of sodium current at more depolarized potentials (−20 to 60 mV). The $\text{Na}_v1.7/\beta_1$ gating parameters, before and after addition of 1 μM PhlTx1 ($n = 4$; Figure 5C), are not affected ($p < 0.05$; see Figure 5D). Again, no alteration in steady-state inactivation or E_{rev} was seen (Figure 5B,E). In order to obtain the IC_{50} value of PhlTx1 on $\text{Na}_v1.7/\beta_1$, expressed in *Xenopus laevis* oocytes, the percentage of toxin-induced block obtained at a stimulus frequency of 0.3 Hz was plotted against the concentration of toxin used and a fit with the Hill equation yielded a value of 260 ± 46 nM with a Hill coefficient = 1.3 (Figure 5F).

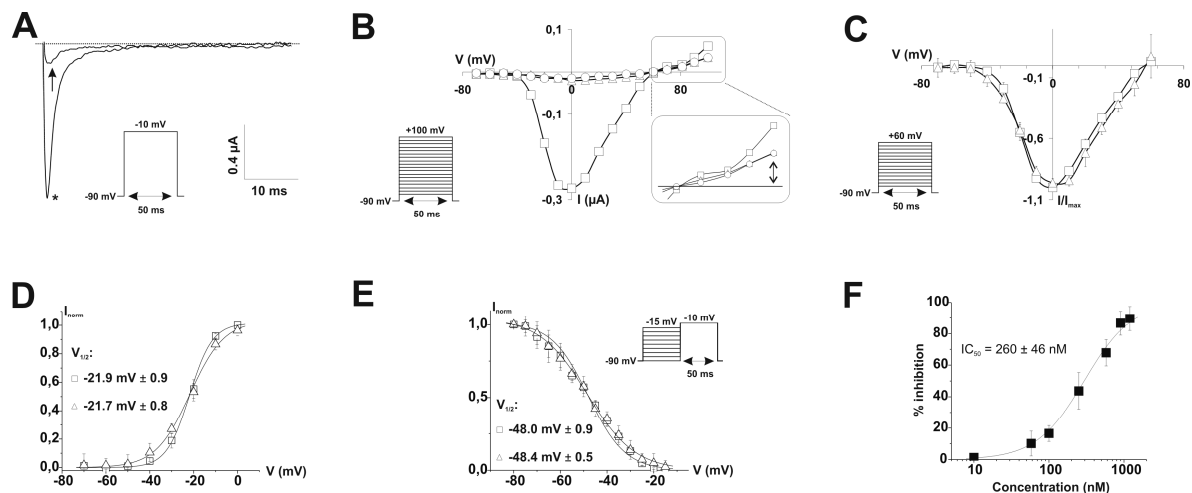


Figure 5. (A) Effect of 1 μM of PhlTx1 on $\text{Na}_v1.7/\beta_1$. Current trace was evoked by a 50-ms depolarization to −10 mV, from a holding potential of −90 mV. A nearly complete block of the inward sodium current is seen (no toxin: *). (B) I–V protocol to positive voltages (+100 mV). \square represents control conditions where no toxin was added. 50 nM of TTX was added (\circ) after maximum block was obtained with 1 μM of PhlTx1 (Δ). No further reduction of the outward current was seen (see inset). Therefore, the remaining outward current does not contain a $\text{Na}_v1.7/\beta_1$ component anymore. (C) Normalized I–V curve of $\text{Na}_v1.7/\beta_1$ before (\square) and after addition of 1 μM PhlTx1 (Δ) ($n = 5$). (D) Normalized activation curves derived from (C). No change in activation voltages or $V_{1/2}$ was seen. (E) Steady-state inactivation curves before and after addition of 1 μM PhlTx1. No effect was seen. (F) In order to obtain the IC_{50} value of PhlTx1 on $\text{Na}_v1.7/\beta_1$, the percentage of toxin-induced block was plotted against the concentration of toxin used and a fit with the Hill equation yielded a value of 260 ± 46 nM ($n = 4$; Hill coefficient = 1.3). The stimulus frequency was 0.3 Hz.

2.4. Refined Affinity of PhlTx1 for the $\text{Na}_v1.7$ Channel in Mammalian Cells

Following our initial screen for the selectivity of synthetic PhlTx1 and the discovery that $\text{Na}_v1.7$ was the main target, we decided to further evaluate the activity of PhlTx1. We used a CHO mammalian cell line expressing the human $\text{Na}_v1.7$ instead of *Xenopus* oocytes for the pharmacological evaluation. To this end, we used an automated patch-clamp system, the Nanion syncropatch 384PE, and a standardized robotic method from Beckmann to apply PhlTx1 in the recording chambers and collect the kinetic information of $\text{Na}_v1.7$ current from a high number of $\text{Na}_v1.7$ -expressing cells. The syncropatch 384PE has the potential to record from 384 cells at a time. 100-ms pulses from −100 mV to −10 mV were applied at a frequency of 0.2 Hz and various concentrations of PhlTx1 were applied to the cells. An example of a $\text{Na}_v1.7$ current recording is illustrated in Figure 6A along with the effect of 100 nM PhlTx1. It is of interest to note that current inhibition develops over time at this PhlTx1 concentration

that is above 50% at the end of a 13-min application time. As in oocytes experiments, PhlTx1 does not affect the kinetics of $\text{Na}_v1.7$ currents (activation or inactivation). We illustrated the time course of current block by PhlTx1 at concentrations (33 nM, 100 nM, 333 nM and 1 μM) that best frame the inhibition of $\text{Na}_v1.7$ -mediated currents (Figure 6B). Note that the highest achievable inhibition was 85%–92% for the two most efficient concentrations (333 nM and 1 μM). The time constant of inhibition was concentration-dependent as expected and could be fitted with decreasing mono-exponentials with time constants of 253 s (33 nM, $n = 4$), 159 s (100 nM, $n = 8$), 97 s (333 nM, $n = 6$) and 36 s (1 μM , $n = 8$). Reporting the maximally reached inhibition at the end of the PhlTx1 application as a function of PhlTx1 concentration indicates that PhlTx1 inhibits $\text{Na}_v1.7$ currents with an IC_{50} value of 39 ± 2 nM (Figure 6C). Using a manual patch clamp, which is better suited to investigate current recovery from block than an automated patch clamp that requires several washing steps, we investigated the reversibility properties of a PhlTx1 block. As shown, the toxin effect was partially and poorly reversible (Figure 6D). After 16 min of washout of 100 nM PhlTx1, we observed a maximum of 32% recovery of the blocked current that occurred with a time constant of 303 s. Since $\text{Na}_v1.4$ and $\text{Na}_v1.6$ were the two most sensitive channels to the PhlTx1 block, we also performed dose-response curves for these two channels with the automated patch clamp system. According to the fits of the data, the calculated IC_{50} values of PhlTx1 for $\text{hNa}_v1.4$ and $\text{hNa}_v1.6$ expressed in CHO and HEK293 cells, respectively, were above 3 μM , indicating that PhlTx1 was indeed quite selective for the human $\text{Na}_v1.7$ channel (Figure 6E,F).

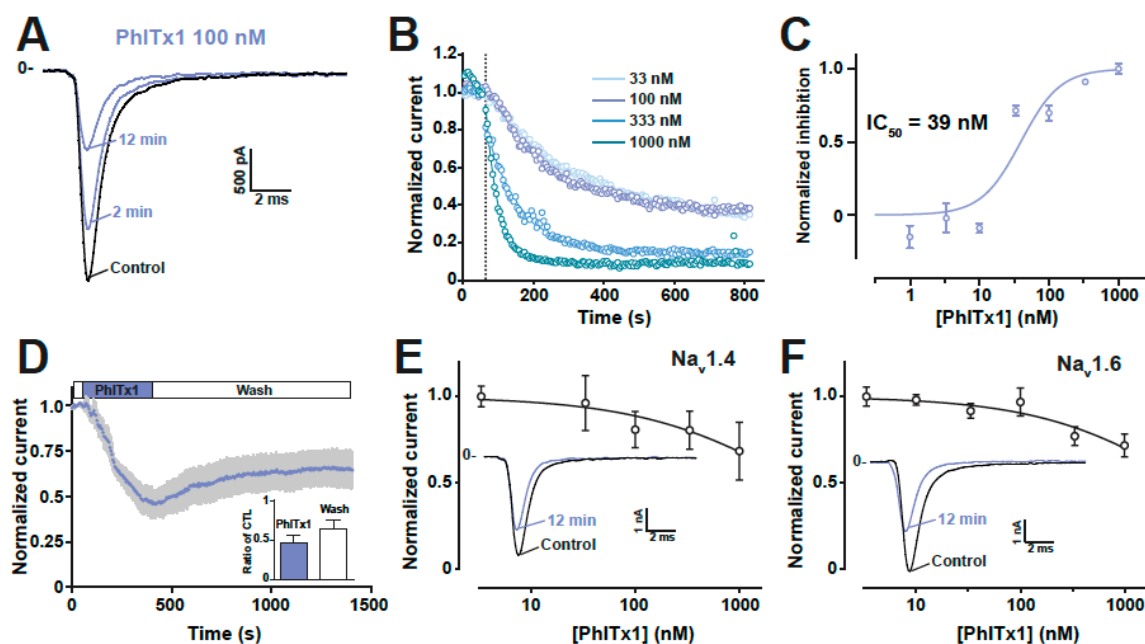


Figure 6. PhlTx1 inhibition of $\text{Na}_v1.7$ channels expressed in a mammalian cell line. (A) Representative current traces of $\text{Na}_v1.7$ current elicited at -10 mV (holding potential = -100 mV) before (Control) and at various times after application of 100 nM PhlTx1 (2 min and 12 min). (B) Average normalized current amplitudes before (left from vertical dotted line) and after application of various concentrations of PhlTx1 (right of dotted line). The average data points were fitted by mono-exponential decay equation $y = 1 - \exp(-t/\tau) + c$ with τ being the time. A c value of 0.09 at 1 μM PhlTx1 indicates that the block induced by PhlTx1 is not complete. A plateau of inhibition was reached for all concentrations. (C) Average dose-response curve of $\text{hNa}_v1.7$ current block by PhlTx1. A sigmoid Hill fit provides an IC_{50} value of 39 ± 2 nM and a Hill value of 1.53. Numbers of cells per concentration: 4 to 8. (D) Average kinetics of reversibility of PhlTx1 block of $\text{hNa}_v1.7$ currents ($n = 5$ cells). (E) Average dose-response curve of hNav1.4 block by PhlTx1. Numbers of cells per concentration: 4 to 13. (F) Average dose-response curve of hNav1.6 block by PhlTx1. Numbers of cells per concentration: 15 to 23.

2.5. Comparison of the $Na_v1.7$ Channel Blocking Efficiency of PhlTx1 with That of Leading Toxins Active on $Na_v1.7$

PhlTx1 has two important properties underpinning its potential to be developed as analgesic: (i) a suitable selectivity profile, and (ii) a high affinity for $Na_v1.7$. Therefore, it was of interest to test how PhlTx1 ranks in terms of $Na_v1.7$ blocking activity compared to some leading peptides that are published as being active on this channel type [50–53]. Comparing data from published information is challenging as often the experiments are performed in different experimental conditions (including different cell lines, different species from which the $Na_v1.7$ clone originates, as well as differing application conditions and chemical synthesis quality, or even if the toxin is of natural or synthetic origin). Thus, we decided to chemically synthesize 10 additional toxins that are reported to block $Na_v1.7$ from various NaSpTx families (1, 2 and 3) and to test them in similar experimental conditions on the CHO cell line expressing $Na_v1.7$. Representative $Na_v1.7$ -mediated currents traces are shown for each toxin type along with the extent of current block by 100 nM of this toxin at two time points (left panels of Figure 7A–J). Several observations can be made. ProTx-I, GsAFI, ProTx-II and HnTx-IV all lead to both relatively rapid and almost a complete block of $Na_v1.7$ current. The average time courses of inhibition are shown on the right panels for a concentration of 100 nM; a concentration set arbitrary that we consider as a good cut-off concentration to decide whether a toxin is an interesting lead blocker for $Na_v1.7$. At this concentration, all toxins block over 50% of the inward current with the exception of Pn3a; this toxin being fully insensitive at this concentration. The block by GrTx1 reached a plateau of inhibition of about 50% on average. The toxins differed also by their time course of block. At 100 nM, the fastest blocking toxins were ProTx-I (double exponential time course of inhibition with time constants of $\tau_1 = 4$ s and $\tau_2 = 114$ s), GsAF1 ($\tau = 21$ s) and GrTx1 ($\tau = 18$ s). Slower, but complete blocks, were observed for HwTx-IV ($\tau = 194$ s), HnTx-III ($\tau = 149$ s), HnTx-IV ($\tau = 62$ s), GsAFII ($\tau = 98$ s) and ProTx-II ($\tau = 72$ s). The slowest blocking toxin was HwTx-I with an incomplete block even after 11 min 20 sec of application ($\tau = 492$ s). The block by GrTx1 was accompanied by a slight current recovery at -10 mV test potential after it reached its maximal block. This is most likely due to a secondary alteration of the voltage-dependence of activation by the toxin, possibly by binding on a second site of lower affinity. This finding is in agreement with the concept of multimodal action of Tarentula toxins developed earlier, including for GrTx1 [54]. Finally, to fully characterize these peptides, we reported the blocking efficacies as a function of toxin concentrations (Figure 7K). The dose-response curves were illustrated for each NaSpTx families (NaSpTx-1: left panel; NaSpTx-2: middle panel; and NaSpTx-3: right panel). As illustrated, within the first family of toxins, PhlTx1 inhibition was most comparable to the inhibition by HnTx-III or HwTx-I (IC_{50} of 39 nM compared to 50.6 nM for HnTx-III or 25.1 nM for HwTx-I). Two toxins outperformed PhlTx1: HnTx-IV with an IC_{50} of 4.3 nM and HwTx-IV with an IC_{50} of 9.6 nM. Within the NaSpTx2 family, ProTx-I was 5.5-fold better than PhlTx1 with an IC_{50} of 7.1 nM, but Pn3a, reportedly very efficient, surprisingly had an estimated IC_{50} of 1457 nM. Within the NaSpTx3 family, all toxins were between 2.6- and 39-fold more active than PhlTx1 (IC_{50} values between 1 nM for GsAFI and 15 nM for GrTx1). The inhibition efficiency of GsAFI was unexpectedly even better than that of ProTx-II, the reference toxin in the literature for blocking $Na_v1.7$ channels. Several of these findings are in contrast with published reports demonstrating the importance of a standardized procedure to properly compare the potency of all these toxins (Table 1).

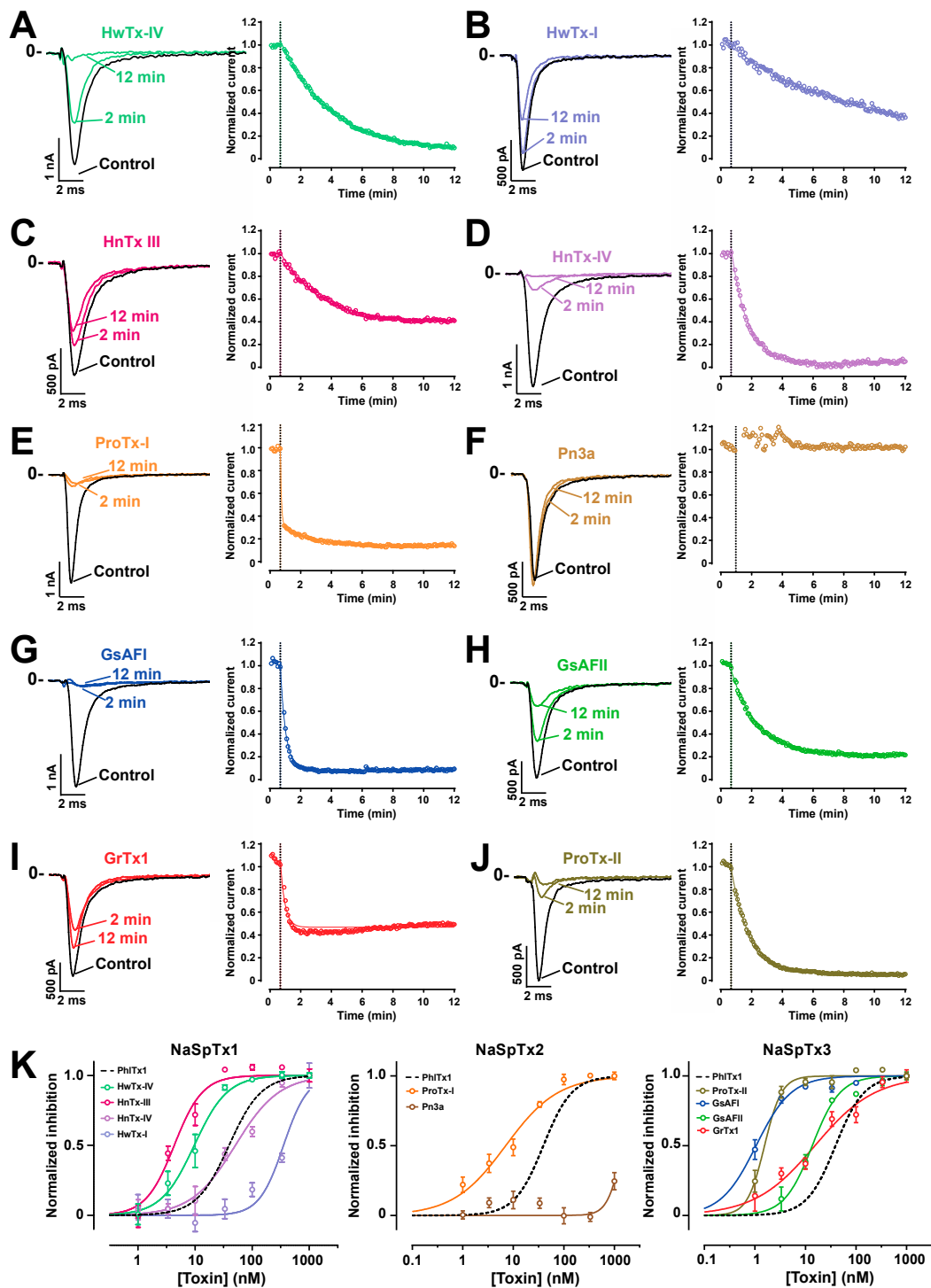


Figure 7. Comparison of PhITx1-mediated inhibition of $Na_v1.7$ currents with the inhibition mediated by other reported $Na_v1.7$ -blocking toxins. (A–J) Ten synthetic toxins, reportedly active on $Na_v1.7$ channel, from three families (NaSpTx1, NaSpTx2 and NaSpTx3) were tested for their blocking potency at 100 nM. Representative traces elicited from a holding potential of -100 mV and test pulse -10 mV in control condition and 2 and 12 min of toxin application time (left panels). All toxins were active at 100 nM with the exception of Pn3a. The kinetic of $Na_v1.7$ current block are shown in the right panels, thereby differentiating the fast and slow blocking toxins at this 100-nM concentration. (K) Normalized dose-response curves of current inhibition of each toxin compared to PhITx1 for each NaSpTx family. Inhibitions were measured at end of a 12- or 15-min application time depending on toxin properties (fast or slow blocking). IC_{50} and Hill values obtained were 7.1 ± 1.2 nM and 0.84 (ProTx-I; $n = 4-8$ cells

per point), 1.0 ± 1.1 nM and 1.2 (GsAFI; $n = 5-8$ cells per point), 13.6 ± 1.2 nM and 1.6 (GsAFII; $n = 2-8$ cells per point), 1.5 ± 1.1 nM and 2.5 (ProTx-II; $n = 5-8$ cells per point), 4.3 ± 1.1 nM and 1.74 (HnTx-IV; $n = 5-8$ cells per point), 15.3 ± 1.2 nM and 0.73 (GrTx1; $n = 5-8$ cells per point), 1457 ± 169 nM and 3 (Pn3a; $n = 3-7$ cells per point), 50.6 ± 1.2 nM and 1.1 (HnTx-III; $n = 5-8$ cells per point), 25.1 ± 1.1 nM and 2.3 (HwTx-I; $n = 2-7$ cells per point), and 9.6 ± 1.2 nM and 1.5 (HwTx-IV; $n = 6-8$ cells per point). IC₅₀ values of HwTx-IV, HwTx-I and HnTx-III are likely to be slightly under-evaluated because of incompletely reaching equilibrium at the lowest effective concentrations. The block by PhlTx1 is shown for comparison (dashed line).

Table 1. Comparison of IC₅₀ values (in nM) for the human Na_v1.7 channel of toxins studied here or published (Publ.) as referenced (Ref.). Published data for GrTx1, GsAFI and GsAFII arise from purified peptides.

Family	NaSpTx1				NaSpTx2			NaSpTx3			
	PhlTx1	HnTx-III	HnTx-IV	HwTx-I	HwTx-IV	ProTx-I	Pn3a	GrTx1	ProTx-II	GsAFI	GsAFII
IC ₅₀	39	50.6	4.3	25.1	9.6	7.1	1457	15.3	1.5	1.0	13.6
Publ.	250	232	21	630	26	72	0.9	370	1	40	1030
Ref.	[47]	[51]	[52]	[55]	[50]	[56]	[45]	[54]	[57]	[54]	[54]

With the exception of ProTx-II, none of the IC₅₀ values we found matched those of the literature. We systematically found better values by an order of 2.7- (HwTx-IV) to 76-fold (GsAFI). The differences in affinity observed for GsAFI, GsAFII and GrTx1 are intriguing. In our analyses, these compounds were 40-, 76- and 25-fold more active in our hands than in an earlier report [54]. Here, two factors may explain the observed differences: (i) lack of use of BSA to avoid non-specific sticking of the peptides to the plastic tubes and dishes, and (ii) the fact that purified peptides were used and not synthetic ones. Quantifying native peptides is more difficult than quantifying synthetic ones because of limited quantities of material and is frequently a source of mistake in defining IC₅₀ values. The 25-fold difference in IC₅₀ value for HwTx-I also demonstrates the importance of standardized protocols for affinity measurements. *A contrario*, the most surprising finding was that Pn3a is far less active than expected [45]. The reason for this discrepancy is unclear, particularly since the chemical synthesis was straightforward. A more in-depth analysis of the disulfide bridge pattern acquired during the synthesis, possibly at odds with what was obtained earlier, may come as an explanation at a later stage.

2.6. Analgesic Potential of PhlTx1 In Vivo

Given the role of Na_v1.7 in nociception, we next evaluated the analgesic activity of PhlTx1 in an inflammatory pain assay on mice and compared the results to those obtained with morphine. Mice were injected intrathecally with vehicle solution only (0.9% NaCl, $n = 11$), morphine (0.25 mg in 10 μ L vehicle, $n = 6$) or toxin-containing solution (100 pmoles PhlTx1 in 10 μ L vehicle, 0.47 μ g/mouse, $n = 5$). Rating of formalin-induced behavior was performed according to the time spent lifting, licking or biting the affected paw. In all cases, no neurotoxicity was observed after intrathecal injection. Strikingly, application of PhlTx1 substantially reduced the response of mice in both the acute pain (Phase I) and inflammation (Phase II) phases induced upon formalin injection into the paw, thereby demonstrating the analgesic effect of the toxin, possibly via a mechanism involving Na_v1.7 inhibition (Figure 8). This is the first formal description of the anti-nociceptive potential of PhlTx1. Although it appears to contradict a previous report suggesting a lack of effect of PhlTx1 on acute pain [45], it must be emphasized that the routes of administration differed (intrathecal here *versus* intraperitoneal in the previous study).

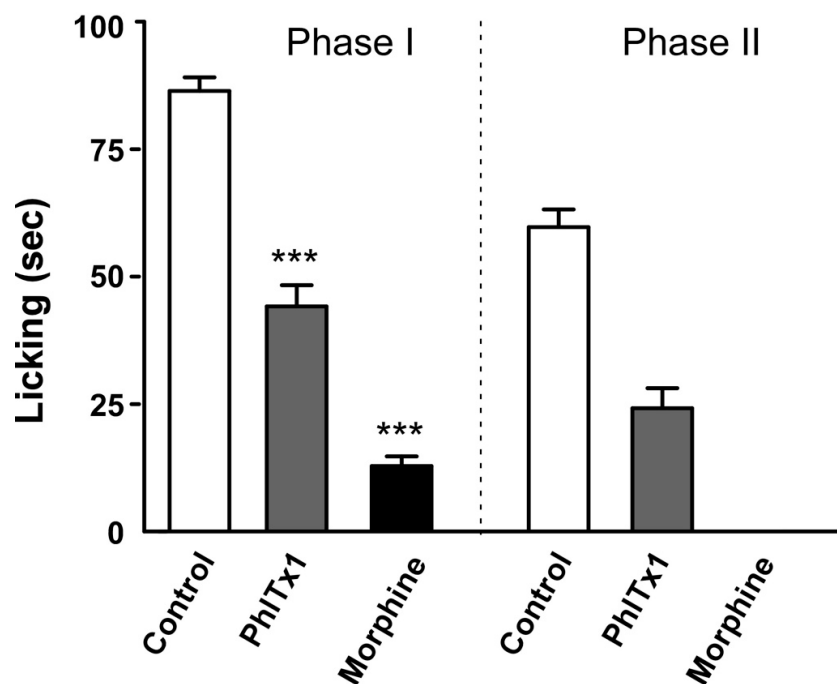


Figure 8. PhlTx1 is effective in a mouse model of acute and inflammatory pain. Effects of PhlTx1 (100 pmoles) and morphine (0.25 mg) on first (0–10 min) and second (10–45 min) phase of formalin-induced spontaneous pain behavior ($n = 6–11$) in mice. The licking value for morphine is 0 during phase II for all mice. Comparisons are *versus* vehicle unless specified. Mean \pm s.e.m. *** = $p < 0.001$. This figure was presented in an earlier meeting in 2006 [47].

3. Discussion

In this report, we illustrated that PhlTx1 is a new member of the NaSpTx-1 family of toxins active on Na_v channels. Since its discovery in 2005, reports on the use of PhlTx1 have been scarce [45,47] and an extensive description of its pharmacology has been lacking. Part of the reason for this lack of published information, at a time where the $\text{Na}_v1.7$ has become a very interesting target for pain treatment, may lie in the difficulties linked to its chemical synthesis. Although the random oxidative folding strategy seems to work, the yields remain largely unsatisfactory to envision any kind of clinical future for this peptide or even to perform a complete Ala scan of the peptide to identify the pharmacophore of PhlTx1. Taking for granted that PhlTx1 folds according to the disulfide bridge motif of the NaSpTx-1 family, we decided to produce the toxin using a directed disulfide bond formation strategy. This strategy ensured that the disulfide bond pattern was respected and unique, led to a better yield of peptide production, and enforced the proper production of toxin variants that otherwise would fail to fold or oxidize properly. Concerning the wild-type sequence of PhlTx1, we do believe however that the random oxidative folding does yield the proper fold and disulfide bridges as both synthetic products coelute.

Although many new toxins are discovered each year, the same questioning regarding the natural target and the potential applications arises systematically. In many cases it is not sufficient to perform a blast search and find some homologous peptides, as this may be insufficient information to determine the target of the toxin. Here, PhlTx1 sequence is quite novel as its sequence barely matches other spider toxins. The fact that PhlTx1 belongs to the NaSpTx-1 family is also not sufficient information to indicate its potential cellular target. For this reason, we performed extensive testing of PhlTx1 activity on several voltage-dependent and one ligand-gated ion channels. Remarkably, we identified $\text{Na}_v1.7$ as the most sensitive ion channel for PhlTx1, with very few additional ion channels being sensitive to this toxin. Two other Na_v channels, $\text{Na}_v1.4$ and $\text{Na}_v1.6$, showed interesting sensitivities as well to PhlTx1, that were better evidenced using mammalian cells than oocytes. The discrepancy in

IC₅₀ value for PhlTx1 blockage observed between oocytes and mammalian cells is a quite common phenomenon. It finds its origin in multiple factors such as lipid composition, the presence or absence of auxiliary subunits, or the fact that oocytes possess an extra vitelline membrane that peptides have to cross to reach their target. The rather narrow selectivity profile places PhlTx1 as an interesting lead candidate for the development of an analgesic. A careful reexamination of its affinity for the human Na_v1.7 channel isoform, expressed in mammalian cells, further reveals that its affinity is below 100-nM. This issue is particularly important if this toxin needs to be further investigated for its analgesic properties considering that its chemical synthesis is not straightforward. High affinity toxins may benefit from the fact that lower amounts need to be used in vivo to become efficient in their therapeutic task.

The modus operandi of channel block by PhlTx1 leads to some thoughts on its potential binding site. At face value, PhlTx1 activity resembles that of TTX that inhibits the pore. Other spider toxins such as HnTx-I, HnTx-III, HnTx-IV, HnTx-V and HwTx-IV also reduce the current amplitude of TTX-sensitive Na_v channels and have therefore been hypothesized to occlude the ion conduction pathway. HnTx-III, HnTx-IV and HnTx-V shift the voltage midpoint of steady-state inactivation to more hyperpolarized potentials, an effect that is not described with TTX when tested in rabbit purkinje fibers or here with PhlTx1. However, it is worth noting that most gating-modifier toxins interact with one or more voltage-sensing domains to inhibit or activate the channel [58]. Therefore, future work on PhlTx1 will include the determination of its binding site.

4. Conclusions

In summary, we successfully synthesized substantial quantities of the tarantula venom toxin PhlTx1 using two unrelated procedures that should greatly facilitate future SAR studies. The synthetic PhlTx1 is biologically active and was shown to predominantly inhibit Na_v1.7-mediated currents in two heterologous expression systems, whereas a large collection of other ion channels is not or only slightly influenced. When tested in a mouse model for inflammatory pain, PhlTx1 reduced the response of mice in the acute pain and inflammation phases, thereby supporting the role of Na_v1.7 in pain perception. Although PhlTx1 is not the most potent Na_v1.7 ligand isolated to date, it is not a weak affinity blocker according to our comparative analyses with leading Na_v1.7 acting toxins. In addition, it can reasonably be assumed that its affinity towards the channel may be improved further. For example, accumulating evidence suggests that defined peptide modifications can result in drastically increased toxin potencies [59–61]. The observation that Na_v1.7 loss-of-function in humans does not induce mortality offers tantalizing prospects for finding new routes of analgesia [19]. PhlTx1, as a selective antagonist of Na_v1.7, should therefore be considered as another exciting lead for novel pain treatments or as a potent pharmacological tool to dissect Na_v1.7 contribution to cellular excitability.

5. Materials and Methods

5.1. Chemicals and Peptides

The following toxins: ProTx-I, ProTx-II, GsAFI, GsAFII, GrTx1, Pn3a, HnTx-III, HnTx-IV, HwTx-I and HwTx-IV were all chemically assembled and provided by Smartox Biotechnology (Saint-Egrève, France).

5.2. Chemical Synthesis of PhlTx1

Linear PhlTx1 was assembled stepwise using fmoc solid-phase chemistry on a Symphony Synthesizer (Protein Technologies Inc., Tucson, AZ, USA) at a 0.1 mmol scale on 2-chlorotrityl chloride resin (substitution approx. 1.6 mmol/g). Fmoc protecting groups were removed using 20% piperidine in dimethylformamid (DMF) and free amine was coupled using tenfold excess of Fmoc amino acids and HCTU/DIEA activation in NMP/DMF (3 times 15 min). For the random oxidative folding strategy, all cysteine residues were introduced with trityl protecting groups. For the directed disulfide bond

formation strategy, Cys² and Cys¹⁷ were introduced with AcM protecting groups, Cys⁹ and Cys²² with trityl protecting groups, and Cys¹⁶ and Cys²⁹ with Mob protecting groups. Linear peptides were deprotected and cleaved from the resin with TFA/H₂O/1,3-dimethoxybenzene/TIS 92.5/2.5/2.5/2.5 (vol.), then precipitated out in cold diethyl ether and the resulting white solids were washed twice with diethyl ether to afford crude linear peptides. Next, for random oxidative folding strategy, the fully deprotected PhITx1 was purified by preparative reversed-phase (RP) HPLC prior to oxidative folding. Purification by RP-HPLC on a C18 (10 µm, 100 Å) Phenomenex Luna stationary phase on an Agilent Technologies preparative HPLC system (eluent system H₂O/MeCN + 0.1% TFA), afforded pure linear PhITx1, which was folded by air oxidation at 0.1 mg/mL in a 100 mM Tris buffer at pH 8.4, containing 5 mM GSH, 0.5 mM GSSG and 2 M Gn.HCl. After 72 hrs at room temperature, the pH of the reaction mixture was adjusted to 3.0 and purified by preparative RP-HPLC. Two purifications, firstly by RP-HPLC on a C18 (10 µm, 100 Å) Phenomenex Luna stationary phase on an Agilent Technologies preparative HPLC system (eluent system H₂O/MeCN + 0.1% TFA), then secondly on a C12 (4 µm, 90 Å) Phenomenex Proteo Jupiter stationary phase on a semi-preparative HPLC system (eluent system H₂O/MeCN + 0.1% TFA), afforded pure synthetic PhITx1 in a 0.25% overall yield. For the directed disulfide bond formation strategy, crude PhITx1 was dissolved in H₂O/MeCN (1:1) at 10 mg/mL and added dropwise to a solution containing 0.1 M citric acid and 10% DMSO, at pH 7.8, to a final peptide concentration of 0.1 mg/mL. After one night under gentle stirring, pH was adjusted to 1–2, and 1 eq. of 50 mM iodine in MeCN was added every five minutes, for a total of five additions. Five minutes after the last addition, the excess of iodine was quenched with sodium ascorbate and the solution was filtered and purified by preparative RP-HPLC. Purification by RP-HPLC on a C18 (10 µm, 100 Å) Phenomenex Luna stationary phase on an Agilent Technologies preparative HPLC system (eluent system H₂O/MeCN + 0.1% TFA) afforded the pure two-disulfide bond PhITx1. The freeze-dried peptide was dissolved in TFA/phenol at 0 °C and TFMSA was added to reach a concentration of 5 mg/mL of peptide in TFA/phenol/TFMSA (8:1:1). The mixture was stirred for 10 min at 0 °C and then the peptide was precipitated out in cold diethyl ether and the resulting white solid was washed twice with diethyl ether. The peptide was dissolved in H₂O/MeCN (1:1) at 10 mg/mL and added dropwise to a solution containing 0.1 M citric acid, 15% DMSO and 2 M Gn.HCl at pH 2.0, to a final peptide concentration of 0.1 mg/mL. After 48 h, the solution was purified by RP-HPLC on a C18 (4 µm, 90 Å) Phenomenex Proteo Jupiter stationary phase on an Agilent Technologies preparative HPLC system (eluent system H₂O/MeCN + 0.1% TFA) to afford pure synthetic PhITx1 in a 1.4% overall yield.

5.3. Cell Culture

CHO cells stably expressing the human Na_v1.7 cells were cultured in Dulbecco's Modified Eagle's Medium (DMEM) supplemented with 10% fetal calf serum, 1 mM pyruvic acid, 4 mM glutamine, 10 IU/mL penicillin and 10 µg/mL streptomycin (Gibco, Grand Island, NY, USA), and incubated at 37 °C in a 5% CO₂ atmosphere. For automated patch-clamp recordings, cells were detached with trypsin and floating single cells were diluted (~300,000 cells/mL) in medium contained (in mM): 4 KCl, 140 NaCl, 5 Glucose, 10 HEPES (pH 7.4, osmolarity 290 mOsm).

5.4. *Xenopus* Oocyte Expression and Recording Experiments

For in vitro transcription, Na_v1.5/pSP64T and Na_v1.8/pSP64T were first linearized with *Xba*I and β₁/pSP64T with *Eco*RI. Capped cRNAs were synthesized from the linearized plasmid using the SP6 mMESSAGE-mMACHINE[®] transcription kit (Ambion, USA). The Na_v1.1/pLCT1, Na_v1.2/pLCT1, Na_v1.3/pNa3T, Na_v1.4/pUI-2, para/pG19-13-5 and tipE/pGH19 vector were linearized with *Not*I and Na_v1.7/pBSTA.rPN1 was linearized with *Sac*II. Transcriptions were performed with the T7 mMESSAGE-mMACHINE[®] kit (ThermoFisher Scientific, Illkirch, France). The harvesting of stage V-VI oocytes from the ovarian lobes of anaesthetized female *Xenopus laevis* frogs was carried out as previously described [62,63]. The use of *Xenopus laevis* was approved by the Animal Care Committee of the University of Leuven. Oocytes were injected with 50 nL of cRNA at a concentration of 1 ng nL⁻¹

using a Drummond (USA) micro-injector. The ND96 solution used for incubating the oocytes contained (in mM): NaCl 96, KCl 2, CaCl₂ 1.8, MgCl₂ 2 and HEPES 5 (pH 7.4), supplemented with 50 mg L⁻¹ gentamycin sulfate and 180 mg L⁻¹ theophyllin. Two-electrode voltage-clamp (TEVC) recordings were performed at room temperature (19–23 °C) using a GeneClamp 500 amplifier (Molecular Devices, USA) controlled by a pClamp data acquisition system (Molecular Devices, USA). Whole-cell currents from oocytes were recorded 2 to 4 days after injection. Voltage and current electrodes were filled with 3 M KCl. Resistances of both electrodes were kept as low as possible (<0.5 MΩ). Bath solution composition was (in mM): NaCl 96, KCl 2, CaCl₂ 1.8, MgCl₂ 2 and HEPES 5 (pH 7.4). Currents were filtered at 1 kHz with a four-pole low-pass Bessel filter, and sampled at 5 kHz. PhlTx1 was dissolved in ND96 containing 0.1% bovine serum albumin (BSA). This stock solution was added to the bath solution at the concentrations indicated. Data manipulation was performed in pClamp8 (Molecular Devices, USA) and Origin software (MVB Scientific, Nes-Ameland, The Netherlands). Averaged data are presented as mean ± SEM. In general, current-voltage relationships (I-V curves) were evoked in oocytes expressing the cloned Na_v channels by 50-ms depolarizations between -70 to +120 mV, using 5 or 10 mV increments from a holding potential of -90 mV. To avoid overestimation of a potential toxin-induced shift in the current-voltage relationship due to inadequate voltage control when measuring large sodium currents in oocytes, only results from cells with currents lower than 1.5 μA were considered. In order to obtain IC₅₀ values, the percentage of toxin-induced block was plotted against the concentration of toxin used. A fit with the Hill equation yielded the IC₅₀ values.

5.5. Pharmacological Applications Using the Automated Patch-Clamp System

PhlTx1 and other Na_v1.7-acting toxins were investigated on CHO cells expressing the human Na_v1.7 channel using the Automated patch-clamp system from Nanion (München, Germany), the SyncroPatch 384PE. Chips with single-hole and high-resistance (~6–7 MΩ) were used for CHO cell recordings. Voltage pulses and whole-cell recordings were achieved using the PatchControl384 v1.5.2 software (Nanion, Munich, Germany) and the Biomek v1.0 interface (Beckman Coulter). Prior recordings, dissociated cells were shaken at 60 RPM in a cell hotel reservoir at 10 °C. After cell catching, sealing, whole-cell formation, liquid application, recording, and data acquisition were all performed sequentially and automatically. The intracellular solution contained (in mM): 10 CsCl, 110 CsF, 10 NaCl, 1 MgCl₂, 1 CaCl₂, 10 EGTA and 10 HEPES (pH 7.2, osmolarity 280 mOsm), and the extracellular solution (in mM): 140 NaCl, 4 KCl, 2 CaCl₂, 1 MgCl₂, 5 Glucose and 10 HEPES (pH 7.4, osmolarity 298 mOsm). Whole-cell experiments were done at -100 mV holding potential and at room temperature (18–22 °C), while currents triggered at -10 mV test potential were sampled at 20 kHz. Stimulation frequency was set at 0.2 Hz. Toxins were prepared at various concentrations in the extracellular solution, itself supplemented with 0.3% BSA. The peptides were distributed in 384-well compound plates according to the number of toxins to be tested (generally four), the concentration range tested according to the assumed IC₅₀ values, and the number of cells desired for each experimental condition. Compound solutions were diluted 3 times in the patch-clamp recording well by adding 30 μL to 60 μL external solution to reach the final reported concentration and the test volume of 90 μL. Percentages of current inhibitions were measured at the end of a 12- to 15-min application time (12-min for fast blocking toxins; 15-min for slow blocking ones). A single concentration of peptide was tested on each cell for building the full-inhibition curves.

5.6. Formalin Pain Test

Pain behavior experiments were performed in C57BL/6J mice with the formalin test which evaluates behavioral responses to subcutaneous injection of 10 μL of 5% formalin into the plantar surface of the right hindpaw. The total time spent in licking and biting the right hindpaw over the next 45 min and divided into two phases (acute phase I, from 0 to 10 min, and inflammatory phase II, from 10 to 45 min) was determined and used as “pain” parameter. The effects of drugs on acute and inflammatory pain were evaluated after intrathecal injection of PhlTx1 (10 μL at 10 μM), or vehicle

(NaCl 0.9%) (10 μ L) or morphine-HCl (Cooper, 10 μ L: 0.25 mg). Data were analyzed with GraphPad Prism 4. After testing the normality of data distribution, the statistical difference between different groups was analyzed using one way Anova followed by a Newman-Keuls multiple comparison test when $p < 0.05$. Mice procedures were approved by the Institutional Local Ethical Committee and authorized by the French Ministry of Research according to the European Union regulations and the Directive 2010/63/EU (Agreements C061525, NCE/2011-06 and 01550.03).

Author Contributions: Conceptualization, M.D.W., J.T., R.B. and D.B.; methodology, S.N., C.Z. and F.B.; software, S.N. and J.M.; validation, D.M., and D.C.; formal analysis, S.N., F.B. and J.M.; investigation, S.N., C.Z., F.B., J.M., S.D., E.C. and S.D.W.; resources, J.T.; data curation, J.T. and M.D.W.; writing—original draft preparation, M.D.W. and J.T.; writing—review and editing, M.D.W.; supervision, D.M., D.C., D.B., M.L., J.T. and M.D.W.; project administration, M.L.; funding acquisition, M.D.W.

Funding: M. De Waard thanks the Agence Nationale de la Recherche (ANR) for its financial support to the laboratory of excellence “Ion Channels, Science and Therapeutics” (grant N° ANR-11-LABX-0015). This work was supported by the Fondation Leducq in the frame of its program of ERPT equipment support (purchase of an automated patch-clamp system), by a grant “New Team” of the Région Pays de la Loire to M. De Waard, and by a European FEDER grant in support of the automated patch-clamp system of Nanion. The salary of S. Nicolas is supported by the Fondation Leducq, while the fellowship of J. Montnach is provided by an ANR Grant to M. De Waard entitled Bradycardia (grant N° ANR-15-CE14-0004-02).

Acknowledgments: We would like to thank the following persons: A.L. Goldin, Univ. of California, Irvine, USA for sharing rNav_v1.1, rNav_v1.2 and rNav_v1.3; G. Mandel, State Univ. of New York, USA for sharing rNav_v1.4; R.G. Kallen, Univ. of Pennsylvania, Philadelphia, USA for sharing hNav_v1.5, Roche (Palo Alto, CA, USA) for sharing hNav_v1.6 and hNav_v1.7; John N. Wood, Univ. College London, UK for sharing rNav_v1.8; S.H. Heinemann, Friedrich-Schiller-Universität Jena, Germany for sharing the β_1 subunit; Martin S. Williamson, IACR-Rothamsted, UK for sharing the DmNav_v1 and tipE clone; and Nanion, Munich, Germany, for sharing the hNav_v1.7 cell line.

Conflicts of Interest: The authors Claude Zoukimian, Rémy Bérout and Michel De Waard declare the following competing interest: employee, CEO and consultant, respectively, of Smartox Biotechnology. The funders had no role in the design of the study; in the collection, analyses, or interpretation of data; in the writing of the manuscript, or in the decision to publish the results.

References

- Dib-Hajj, S.D.; Cummins, T.R.; Black, J.A.; Waxman, S.G. Sodium channels in normal and pathological pain. *Annu. Rev. Neurosci.* **2010**, *33*, 325–347. [[CrossRef](#)] [[PubMed](#)]
- Faber, C.G.; Lauria, G.; Merkies, I.S.; Cheng, X.; Han, C.; Ahn, H.S.; Persson, A.K.; Hoeijmakers, J.G.; Gerrits, M.M.; Pierro, T.; et al. Gain-of-function Nav1.8 mutations in painful neuropathy. *Proc. Natl. Acad. Sci. USA* **2012**, *109*, 19444–19449. [[CrossRef](#)] [[PubMed](#)]
- Hille, B. *Ion Channels of Excitable Membranes*, 3rd ed.; Sinauer Associates Inc.: Sunderland, MA, USA, 2001; Volume 1.
- Leipold, E.; Liebmann, L.; Korenke, G.C.; Heinrich, T.; Giesselmann, S.; Baets, J.; Ebbinghaus, M.; Goral, R.O.; Stodberg, T.; Hennings, J.C.; et al. A de novo gain-of-function mutation in SCN11A causes loss of pain perception. *Nat. Genet.* **2013**, *45*, 1399–1404. [[CrossRef](#)] [[PubMed](#)]
- Ahern, C.A.; Payandeh, J.; Bosmans, F.; Chanda, B. The hitchhiker’s guide to the voltage-gated sodium channel galaxy. *J. Gen. Physiol.* **2016**, *147*, 1–24. [[CrossRef](#)] [[PubMed](#)]
- Bregman, H.; Berry, L.; Buchanan, J.L.; Chen, A.; Du, B.; Feric, E.; Hierl, M.; Huang, L.; Immke, D.; Janosky, B.; et al. Identification of a potent, state-dependent inhibitor of Nav1.7 with oral efficacy in the formalin model of persistent pain. *J. Med. Chem.* **2011**, *54*, 4427–4445. [[CrossRef](#)] [[PubMed](#)]
- Chakka, N.; Bregman, H.; Du, B.; Nguyen, H.N.; Buchanan, J.L.; Feric, E.; Ligutti, J.; Liu, D.; McDermott, J.S.; Zou, A.; et al. Discovery and hit-to-lead optimization of pyrrolopyrimidines as potent, state-dependent Na(v)1.7 antagonists. *Bioorg. Med. Chem. Lett.* **2012**, *22*, 2052–2062. [[CrossRef](#)] [[PubMed](#)]
- Focken, T.; Liu, S.; Chahal, N.; Dauphinais, M.; Grimwood, M.E.; Chowdhury, S.; Hemeon, I.; Bichler, P.; Bogucki, D.; Waldbrook, M.; et al. Discovery of Aryl Sulfonamides as Isoform-Selective Inhibitors of Nav1.7 with Efficacy in Rodent Pain Models. *ACS Med. Chem. Lett.* **2016**, *7*, 277–282. [[CrossRef](#)]
- Frost, J.M.; DeGoey, D.A.; Shi, L.; Gum, R.J.; Fricano, M.M.; Lundgaard, G.L.; El-Kouhen, O.F.; Hsieh, G.C.; Neelands, T.; Matulenko, M.A.; et al. Substituted Indazoles as Nav1.7 Blockers for the Treatment of Pain. *J. Med. Chem.* **2016**, *59*, 3373–3391. [[CrossRef](#)]

10. Graceffa, R.F.; Boezio, A.A.; Able, J.; Altmann, S.; Berry, L.M.; Boezio, C.; Butler, J.R.; Chu-Moyer, M.; Cooke, M.; DiMauro, E.F.; et al. Sulfonamides as Selective Nav1.7 Inhibitors: Optimizing Potency, Pharmacokinetics, and Metabolic Properties to Obtain Atropisomeric Quinolinone (AM-0466) that Affords Robust in Vivo Activity. *J. Med. Chem.* **2017**, *60*, 5990–6017. [[CrossRef](#)]
11. Ho, G.D.; Tulshian, D.; Bercovici, A.; Tan, Z.; Hanisak, J.; Brumfield, S.; Matasi, J.; Heap, C.R.; Earley, W.G.; Courneya, B.; et al. Discovery of pyrrolo-benzo-1,4-diazines as potent Na(v)1.7 sodium channel blockers. *Bioorg. Med. Chem. Lett.* **2014**, *24*, 4110–4113. [[CrossRef](#)]
12. Macsari, I.; Besidski, Y.; Csjernyik, G.; Nilsson, L.I.; Sandberg, L.; Yngve, U.; Ahlin, K.; Bueters, T.; Eriksson, A.B.; Lund, P.E.; et al. 3-Oxoisoindoline-1-carboxamides: Potent, state-dependent blockers of voltage-gated sodium channel Na(V)1.7 with efficacy in rat pain models. *J. Med. Chem.* **2012**, *55*, 6866–6880. [[CrossRef](#)] [[PubMed](#)]
13. Marx, I.E.; Dineen, T.A.; Able, J.; Bode, C.; Bregman, H.; Chu-Moyer, M.; DiMauro, E.F.; Du, B.; Foti, R.S.; Freneau, R.T., Jr.; et al. Sulfonamides as Selective Nav1.7 Inhibitors: Optimizing Potency and Pharmacokinetics to Enable in Vivo Target Engagement. *ACS Med. Chem. Lett.* **2016**, *7*, 1062–1067. [[CrossRef](#)] [[PubMed](#)]
14. Nguyen, H.N.; Bregman, H.; Buchanan, J.L.; Du, B.; Feric, E.; Huang, L.; Li, X.; Ligutti, J.; Liu, D.; Malmberg, A.B.; et al. Discovery and optimization of aminopyrimidinones as potent and state-dependent Nav1.7 antagonists. *Bioorg. Med. Chem. Lett.* **2012**, *22*, 1055–1060. [[CrossRef](#)] [[PubMed](#)]
15. Roecker, A.J.; Egbertson, M.; Jones, K.L.G.; Gomez, R.; Kraus, R.L.; Li, Y.; Koser, A.J.; Urban, M.O.; Klein, R.; Clements, M.; et al. Discovery of selective, orally bioavailable, N-linked arylsulfonamide Nav1.7 inhibitors with pain efficacy in mice. *Bioorg. Med. Chem. Lett.* **2017**, *27*, 2087–2093. [[CrossRef](#)] [[PubMed](#)]
16. Sun, S.; Jia, Q.; Zenova, A.Y.; Chafeev, M.; Zhang, Z.; Lin, S.; Kwan, R.; Grimwood, M.E.; Chowdhury, S.; Young, C.; et al. The discovery of benzenesulfonamide-based potent and selective inhibitors of voltage-gated sodium channel Na(v)1.7. *Bioorg. Med. Chem. Lett.* **2014**, *24*, 4397–4401. [[CrossRef](#)]
17. Suzuki, S.; Kuroda, T.; Kimoto, H.; Domon, Y.; Kubota, K.; Kitano, Y.; Yokoyama, T.; Shimizugawa, A.; Sugita, R.; Koishi, R.; et al. Discovery of (phenoxy-2-hydroxypropyl)piperidines as a novel class of voltage-gated sodium channel 1.7 inhibitors. *Bioorg. Med. Chem. Lett.* **2015**, *25*, 5419–5423. [[CrossRef](#)] [[PubMed](#)]
18. Wu, W.; Li, Z.; Yang, G.; Teng, M.; Qin, J.; Hu, Z.; Hou, L.; Shen, L.; Dong, H.; Zhang, Y.; et al. The discovery of tetrahydropyridine analogs as hNav1.7 selective inhibitors for analgesia. *Bioorg. Med. Chem. Lett.* **2017**, *27*, 2210–2215. [[CrossRef](#)]
19. Cox, J.J.; Reimann, F.; Nicholas, A.K.; Thornton, G.; Roberts, E.; Springell, K.; Karbani, G.; Jafri, H.; Mannan, J.; Raashid, Y.; et al. An SCN9A channelopathy causes congenital inability to experience pain. *Nature* **2006**, *444*, 894–898. [[CrossRef](#)]
20. Nassar, M.A.; Stirling, L.C.; Forlani, G.; Baker, M.D.; Matthews, E.A.; Dickenson, A.H.; Wood, J.N. Nociceptor-specific gene deletion reveals a major role for Nav1.7 (PN1) in acute and inflammatory pain. *Proc. Natl. Acad. Sci. USA* **2004**, *101*, 12706–12711. [[CrossRef](#)]
21. Gingras, J.; Smith, S.; Matson, D.J.; Johnson, D.; Nye, K.; Couture, L.; Feric, E.; Yin, R.; Moyer, B.D.; Peterson, M.L.; et al. Global Nav1.7 knockout mice recapitulate the phenotype of human congenital indifference to pain. *PLoS ONE* **2014**, *9*, e105895. [[CrossRef](#)]
22. Fertleman, C.R.; Baker, M.D.; Parker, K.A.; Moffatt, S.; Elmslie, F.V.; Abrahamsen, B.; Ostman, J.; Klugbauer, N.; Wood, J.N.; Gardiner, R.M.; et al. SCN9A mutations in paroxysmal extreme pain disorder: Allelic variants underlie distinct channel defects and phenotypes. *Neuron* **2006**, *52*, 767–774. [[CrossRef](#)] [[PubMed](#)]
23. Hoeijmakers, J.G.; Han, C.; Merkies, I.S.; Macala, L.J.; Lauria, G.; Gerrits, M.M.; Dib-Hajj, S.D.; Faber, C.G.; Waxman, S.G. Small nerve fibres, small hands and small feet: A new syndrome of pain, dysautonomia and acromesomelia in a kindred with a novel Nav1.7 mutation. *Brain* **2012**, *135*, 345–358. [[CrossRef](#)] [[PubMed](#)]
24. Bennett, D.L.; Clark, A.J.; Huang, J.; Waxman, S.G.; Dib-Hajj, S.D. The Role of Voltage-Gated Sodium Channels in Pain Signaling. *Physiol. Rev.* **2019**, *99*, 1079–1151. [[CrossRef](#)] [[PubMed](#)]
25. Faber, C.G.; Hoeijmakers, J.G.; Ahn, H.S.; Cheng, X.; Han, C.; Choi, J.S.; Estacion, M.; Lauria, G.; Vanhoutte, E.K.; Gerrits, M.M.; et al. Gain of function Nanu1.7 mutations in idiopathic small fiber neuropathy. *Ann. Neurol.* **2012**, *71*, 26–39. [[CrossRef](#)] [[PubMed](#)]
26. Cummins, T.R.; Dib-Hajj, S.D.; Waxman, S.G. Electrophysiological properties of mutant Nav1.7 sodium channels in a painful inherited neuropathy. *J. Neurosci.* **2004**, *24*, 8232–8236. [[CrossRef](#)]

27. Dib-Hajj, S.D.; Rush, A.M.; Cummins, T.R.; Hisama, F.M.; Novella, S.; Tyrrell, L.; Marshall, L.; Waxman, S.G. Gain-of-function mutation in Nav1.7 in familial erythromelalgia induces bursting of sensory neurons. *Brain* **2005**, *128*, 1847–1854. [[CrossRef](#)]
28. Fischer, T.Z.; Waxman, S.G. Familial pain syndromes from mutations of the Nav1.7 sodium channel. *Ann. N. Y. Acad. Sci.* **2010**, *1184*, 196–207. [[CrossRef](#)]
29. Chen, B.; Zhang, C.; Wang, Z.; Chen, Y.; Xie, H.; Li, S.; Liu, X.; Liu, Z.; Chen, P. Mechanistic insights into Nav1.7-dependent regulation of rat prostate cancer cell invasiveness revealed by toxin probes and proteomic analysis. *FEBS J.* **2019**. [[CrossRef](#)]
30. Yildirim, S.; Altun, S.; Gumushan, H.; Patel, A.; Djamgoz, M.B. Voltage-gated sodium channel activity promotes prostate cancer metastasis in vivo. *Cancer Lett.* **2012**, *323*, 58–61. [[CrossRef](#)]
31. Kis-Toth, K.; Hajdu, P.; Bacskai, I.; Szilagyi, O.; Papp, F.; Szanto, A.; Posta, E.; Gogolak, P.; Panyi, G.; Rajnavolgyi, E. Voltage-gated sodium channel Nav1.7 maintains the membrane potential and regulates the activation and chemokine-induced migration of a monocyte-derived dendritic cell subset. *J. Immunol.* **2011**, *187*, 1273–1280. [[CrossRef](#)]
32. Muroi, Y.; Ru, F.; Kollarik, M.; Canning, B.J.; Hughes, S.A.; Walsh, S.; Sigg, M.; Carr, M.J.; Undem, B.J. Selective silencing of Na(V)1.7 decreases excitability and conduction in vagal sensory neurons. *J. Physiol.* **2011**, *589*, 5663–5676. [[CrossRef](#)] [[PubMed](#)]
33. Weiss, J.; Pyrski, M.; Jacobi, E.; Bufe, B.; Willnecker, V.; Schick, B.; Zizzari, P.; Gossage, S.J.; Greer, C.A.; Leinders-Zufall, T.; et al. Loss-of-function mutations in sodium channel Nav1.7 cause anosmia. *Nature* **2011**, *472*, 186–190. [[CrossRef](#)] [[PubMed](#)]
34. Goldberg, Y.P.; Price, N.; Namdari, R.; Cohen, C.J.; Lamers, M.H.; Winters, C.; Price, J.; Young, C.E.; Verschoof, H.; Sherrington, R.; et al. Treatment of Na(v)1.7-mediated pain in inherited erythromelalgia using a novel sodium channel blocker. *Pain* **2012**, *153*, 80–85. [[CrossRef](#)] [[PubMed](#)]
35. Hoyt, S.B.; London, C.; Abbadie, C.; Felix, J.P.; Garcia, M.L.; Jochnowitz, N.; Karanam, B.V.; Li, X.; Lyons, K.A.; McGowan, E.; et al. A novel benzazepinone sodium channel blocker with oral efficacy in a rat model of neuropathic pain. *Bioorg. Med. Chem. Lett.* **2013**, *23*, 3640–3645. [[CrossRef](#)] [[PubMed](#)]
36. Ahuja, S.; Mukund, S.; Deng, L.; Khakh, K.; Chang, E.; Ho, H.; Shriver, S.; Young, C.; Lin, S.; Johnson, J.P., Jr.; et al. Structural basis of Nav1.7 inhibition by an isoform-selective small-molecule antagonist. *Science* **2015**, *350*, aac5464. [[CrossRef](#)] [[PubMed](#)]
37. Bosmans, F.; Swartz, K.J. Targeting voltage sensors in sodium channels with spider toxins. *Trends Pharmacol. Sci.* **2010**, *31*, 175–182. [[CrossRef](#)] [[PubMed](#)]
38. Catterall, W.A.; Cestele, S.; Yarov-Yarovoy, V.; Yu, F.H.; Konoki, K.; Scheuer, T. Voltage-gated ion channels and gating modifier toxins. *Toxicon* **2007**, *49*, 124–141. [[CrossRef](#)]
39. Gilchrist, J.; Bosmans, F. Animal toxins can alter the function of Nav1.8 and Nav1.9. *Toxins* **2012**, *4*, 620–632. [[CrossRef](#)]
40. Catterall, W.A.; Goldin, A.L.; Waxman, S.G. International Union of Pharmacology. XLVII. Nomenclature and structure-function relationships of voltage-gated sodium channels. *Pharmacol. Rev.* **2005**, *57*, 397–409. [[CrossRef](#)]
41. Payandeh, J.; Scheuer, T.; Zheng, N.; Catterall, W.A. The crystal structure of a voltage-gated sodium channel. *Nature* **2011**, *475*, 353–358. [[CrossRef](#)]
42. Schmalhofer, W.A.; Calhoun, J.; Burrows, R.; Bailey, T.; Kohler, M.G.; Weinglass, A.B.; Kaczorowski, G.J.; Garcia, M.L.; Koltzenburg, M.; Priest, B.T. ProTx-II, a selective inhibitor of Nav1.7 sodium channels, blocks action potential propagation in nociceptors. *Mol. Pharmacol.* **2008**, *74*, 1476–1484. [[CrossRef](#)] [[PubMed](#)]
43. Maertens, C.; Cuypers, E.; Amininasab, M.; Jalali, A.; Vatanpour, H.; Tytgat, J. Potent modulation of the voltage-gated sodium channel Nav1.7 by OD1, a toxin from the scorpion *Odontobuthus doriae*. *Mol. Pharmacol.* **2006**, *70*, 405–414. [[CrossRef](#)]
44. Yang, S.; Xiao, Y.; Kang, D.; Liu, J.; Li, Y.; Undheim, E.A.; Klint, J.K.; Rong, M.; Lai, R.; King, G.F. Discovery of a selective Nav1.7 inhibitor from centipede venom with analgesic efficacy exceeding morphine in rodent pain models. *Proc. Natl. Acad. Sci. USA* **2013**, *110*, 17534–17539. [[CrossRef](#)] [[PubMed](#)]
45. Deuis, J.R.; Dekan, Z.; Wingerd, J.S.; Smith, J.J.; Munasinghe, N.R.; Bhola, R.F.; Imlach, W.L.; Herzig, V.; Armstrong, D.A.; Rosengren, K.J.; et al. Pharmacological characterisation of the highly Nav1.7 selective spider venom peptide Pn3a. *Sci. Rep.* **2017**, *7*, 40883. [[CrossRef](#)] [[PubMed](#)]

46. Goncalves, T.C.; Benoit, E.; Partiseti, M.; Servent, D. The NaV1.7 Channel Subtype as an Antinociceptive Target for Spider Toxins in Adult Dorsal Root Ganglia Neurons. *Front. Pharmacol.* **2018**, *9*, 1000. [[CrossRef](#)]
47. Bosmans, F.; Escoubas, P.; Diochot, S.; Mebs, D.; Craik, D.; Hill, J.; Nakajima, T.; Lazdunski, M.; Tytgat, J. Isolation and characterization of phlotoxin 1 (PhlTx1), a novel peptide active on voltage-gated sodium channels. In Proceedings of the 13^{ème} Rencontres en Toxinologie “Toxines et douleur”, Paris, France, 1–2 December 2005.
48. Emery, E.C.; Luiz, A.P.; Wood, J.N. Nav1.7 and other voltage-gated sodium channels as drug targets for pain relief. *Expert Opin. Ther. Targets* **2016**, *20*, 975–983. [[CrossRef](#)] [[PubMed](#)]
49. Blacklow, B.; Kornhauser, R.; Hains, P.G.; Loiacono, R.; Escoubas, P.; Gaudins, A.; Nicholson, G.M. alpha-Elapitoxin-Aa2a, a long-chain snake alpha-neurotoxin with potent actions on muscle (alpha1)(2)betagammadelta nicotinic receptors, lacks the classical high affinity for neuronal alpha7 nicotinic receptors. *Biochem. Pharmacol.* **2011**, *81*, 314–325. [[CrossRef](#)]
50. Xiao, Y.; Bingham, J.P.; Zhu, W.; Moczydlowski, E.; Liang, S.; Cummins, T.R. Tarantula huwentoxin-IV inhibits neuronal sodium channels by binding to receptor site 4 and trapping the domain ii voltage sensor in the closed configuration. *J. Biol. Chem.* **2008**, *283*, 27300–27313. [[CrossRef](#)]
51. Liu, Z.; Cai, T.; Zhu, Q.; Deng, M.; Li, J.; Zhou, X.; Zhang, F.; Li, D.; Li, J.; Liu, Y.; et al. Structure and function of hainantoxin-III, a selective antagonist of neuronal tetrodotoxin-sensitive voltage-gated sodium channels isolated from the Chinese bird spider *Ornithoctonus hainana*. *J. Biol. Chem.* **2013**, *288*, 20392–20403. [[CrossRef](#)]
52. Liu, Y.; Tang, J.; Zhang, Y.; Xun, X.; Tang, D.; Peng, D.; Yi, J.; Liu, Z.; Shi, X. Synthesis and analgesic effects of mu-TRTX-Hhn1b on models of inflammatory and neuropathic pain. *Toxins* **2014**, *6*, 2363–2378. [[CrossRef](#)]
53. Klint, J.K.; Smith, J.J.; Vetter, I.; Rupasinghe, D.B.; Er, S.Y.; Senff, S.; Herzig, V.; Mobli, M.; Lewis, R.J.; Bosmans, F.; et al. Seven novel modulators of the analgesic target NaV 1.7 uncovered using a high-throughput venom-based discovery approach. *Br. J. Pharmacol.* **2015**, *172*, 2445–2458. [[CrossRef](#)]
54. Redaelli, E.; Cassulini, R.R.; Silva, D.F.; Clement, H.; Schiavon, E.; Zamudio, F.Z.; Odell, G.; Arcangeli, A.; Clare, J.J.; Alagon, A.; et al. Target promiscuity and heterogeneous effects of tarantula venom peptides affecting Na⁺ and K⁺ ion channels. *J. Biol. Chem.* **2010**, *285*, 4130–4142. [[CrossRef](#)] [[PubMed](#)]
55. Meng, E.; Cai, T.F.; Li, W.Y.; Zhang, H.; Liu, Y.B.; Peng, K.; Liang, S.; Zhang, D.Y. Functional expression of spider neurotoxic peptide huwentoxin-I in *E. coli*. *PLoS ONE* **2011**, *6*, e21608. [[CrossRef](#)]
56. Middleton, R.E.; Warren, V.A.; Kraus, R.L.; Hwang, J.C.; Liu, C.J.; Dai, G.; Brochu, R.M.; Kohler, M.G.; Gao, Y.D.; Garsky, V.M.; et al. Two tarantula peptides inhibit activation of multiple sodium channels. *Biochemistry* **2002**, *41*, 14734–14747. [[CrossRef](#)]
57. Park, J.H.; Carlin, K.P.; Wu, G.; Ilyin, V.I.; Musza, L.L.; Blake, P.R.; Kyle, D.J. Studies examining the relationship between the chemical structure of protoxin II and its activity on voltage gated sodium channels. *J. Med. Chem.* **2014**, *57*, 6623–6631. [[CrossRef](#)] [[PubMed](#)]
58. Bosmans, F.; Martin-Eauclaire, M.F.; Swartz, K.J. Deconstructing voltage sensor function and pharmacology in sodium channels. *Nature* **2008**, *456*, 202–208. [[CrossRef](#)] [[PubMed](#)]
59. Chi, V.; Pennington, M.W.; Norton, R.S.; Tarcha, E.J.; Londono, L.M.; Sims-Fahey, B.; Upadhyay, S.K.; Lakey, J.T.; Iadonato, S.; Wulff, H.; et al. Development of a sea anemone toxin as an immunomodulator for therapy of autoimmune diseases. *Toxicon* **2012**, *59*, 529–546. [[CrossRef](#)]
60. Craik, D.J.; Adams, D.J. Chemical modification of conotoxins to improve stability and activity. *ACS Chem. Biol.* **2007**, *2*, 457–468. [[CrossRef](#)]
61. Han, T.S.; Teichert, R.W.; Olivera, B.M.; Bulaj, G. Conus venoms—A rich source of peptide-based therapeutics. *Curr. Pharm. Des.* **2008**, *14*, 2462–2479. [[CrossRef](#)]
62. Altafaj, X.; Joux, N.; Ronjat, M.; De Waard, M. Oocyte expression with injection of purified T7 RNA polymerase. *Methods Mol. Biol.* **2006**, *322*, 55–67. [[CrossRef](#)]
63. Geib, S.; Sandoz, G.; Carlier, E.; Cornet, V.; Cheynet-Sauvion, V.; De Waard, M. A novel *Xenopus* oocyte expression system based on cytoplasmic coinjection of T7-driven plasmids and purified T7-RNA polymerase. *Recept. Channels* **2001**, *7*, 331–343. [[PubMed](#)]

